CrystEngComm

ROYAL SOCIETY OF CHEMISTRY

PAPER

View Article Online
View Journal | View Issue

Cite this: *CrystEngComm*, 2021, **23**, 6761

Metastable growth and infrared spectra of CuB_2O_4:Ni single crystals†

Evgeniya Moshkina, [a] Maxim Molokeev,[abc] Nadejda Belskaya, *[ad] Ivan Nemtsev,[abe] Anastasiia Molchanova[f] and Kirill Boldyrev [f]

Received 3rd June 2021,
Accepted 18th August 2021

DOI: 10.1039/d1ce00729g

rsc.li/crystengcomm

In this work, the formation of CuB_2O_4:Ni crystals in fluxes based on Li_2WO_4–Bi_2O_3–WO_3 solvents was studied. The crystallized phases were studied with respect to the WO_3 content and the mode of crystal holder insertion. A distinctive feature of the used flux growing mode is the metastable nature of nucleation: the desirable phase was obtained by using a super-cooled crystal holder – under insertion of a crystal holder cooled down to temperatures of the metastable zone. By powder X-ray diffraction, the composition of the obtained samples was analyzed. IR reflection and transmission spectra of the as-synthesized single crystals were recorded and analyzed in comparison with that of "pure" CuB_2O_4.

Introduction

The first works devoted to the preparation and study of CuB_2O_4 metaborate properties date back to the beginning of the last century.[1,2] As of now, there are over one hundred papers published in highly rated scientific journals. These papers are devoted to the study of this unique compound possessing a complex magnetic phase diagram,[3–5] demonstrating the impressive dependence of optical constants on the direction of light propagation (which manifests itself only in systems with violated parity),[6–9] in particular strong photoluminescence that highlights CuB_2O_4 as the first Cu^{2+}-containing magnetically ordered material with such a strong signal.[10]

CuB_2O_4 has a unique noncentrosymmetric crystal structure and characterized by a piezoelectric tetragonal space group $I\bar{4}2d$ (no. 122). The unit cell contains 12 formula units, and Cu^{2+} cations occupy two nonequivalent positions 4*b* and 8*d*.[3] Despite the existence of CoB_2O_4 and MnB_2O_4, they are not isomorphic to CuB_2O_4.[11] Unlike $Mn^{2+}$and Co^{2+}, Cu^{2+} has a pronounced Jahn–Teller effect. However, there are compounds with partial substitution of Cu^{2+} cations by Co^{2+}, Mn^{2+} and Ni^{2+} preserving the symmetry of the initial CuB_2O_4 metaborate.[11–13]

The magnetic phase diagram of CuB_2O_4 includes 6 magnetic phase transitions in a zero magnetic field. There are two magnetic subsystems formed by copper ions located at two nonequivalent crystallographic positions (4*b* and 8*d*).[3] At T_N = 21 K, the ordering of the Cu (4*b*) subsystem into a commensurate antiferromagnetic structure occurs. As the temperature decreases, two successive phase transitions to the incommensurate helical structure at T_1^* = 8.5 K and T_2^* = 7.9 K take place. The phase transitions are caused by the successive re-orientations of the major axis of the ellipse by 90° (a helical structure is elliptic in this case).[3] Recently, the low temperature range of the phase diagram has been studied at $T < 2$ K. Three more magnetic phase transitions were detected in the zero magnetic field: T_3 = 2.02 K and T_4 = 2 K – magnetic phase transitions between two elliptical magnetic structures, the major axes of which ellipses make an angle of 90°; T_5 = 1.85 K – magnetic phase transition to a simple helical structure. The Cu (8*d*) magnetic subsystem is quasi-one-dimensional and remains disordered even at low temperatures.[3]

There is no information in the literature on the magnetoelectric properties of CuB_2O_4; however, it was shown that the partial substitution of nickel for copper (~3%) leads to a significant increase in magnetization and the appearance of electric polarization under the action of a magnetic field.[13] It was also demonstrated that it is possible to control the magnetization of nickel-doped copper metaborate using an electric field.[14] In other words, (Cu, Ni)B_2O_4 is a multiferroic. Thus, it is interesting to study and characterize crystals (Cu, Ni)B_2O_4 containing different percentages of Ni.

[a] *Kirensky Institute of Physics SB RAS, 660036 Krasnoyarsk, Russia. E-mail: nadejda-bels@mail.ru*
[b] *Siberian Federal University, 660041 Krasnoyarsk, Russia*
[c] *Department of Physics, Far Eastern State Transport University, Khabarovsk 680021, Russia*
[d] *Reshetnev Siberian State University of Science and Technology, 660037 Krasnoyarsk, Russia*
[e] *Federal Research Center "Krasnoyarsk Science Center of the Siberian Branch of the Russian Academy of Sciences", 660036 Krasnoyarsk, Russia*
[f] *Institute of Spectroscopy RAS, 108840 Troitsk, Moscow, Russia*

† Electronic supplementary information (ESI) available. CCDC 2084362 and 2084363. For ESI and crystallographic data in CIF or other electronic format see DOI: 10.1039/d1ce00729g

Many experimental CuB_2O_4 studies presented in print are performed using single crystals grown by a flux method. The solvents based on B_2O_3,[15] Li_2O–B_2O_3,[16,17] Bi_2O_3–B_2O_3,[18] and $Bi_2Mo_3O_{12}$[18] have been used. The most vivid result of the growth experiments is the single crystal of CuB_2O_4 with a mass $m \approx 70$ g obtained by the Kyropoulos method from the flux based on $Bi_2Mo_3O_{12}$ (the growing has been carried out in the near-surface layer by gradual "pulling" of the grown part out of the flux).[18] Choosing of the growth method is caused by the near-surface character of nucleation in this flux. This could be accounted for due to the lower density of the crystal than the flux.

In the present work, the results of growth experiments aimed at obtaining $Cu_{1-x}Ni_xB_2O_4$ (x = 0.001 and 0.01) single crystals are presented. Using another solvent type, we tried to study and change the conditions to solve the problem of near-surface nucleation. Different approaches are suggested for CuB_2O_4:Ni crystallization. One of the work's features is the specific character of the metaborate crystal nucleation using a super-cooled crystal holder. The work presents the influence of nickel doping to optical IR spectra.

Crystal growth

The traditional technique of flux crystal growth in a mode of spontaneous nucleation using a crystal holder involves the dissolution of crystal forming components (oxides in our case) in the solvent at temperatures which are quite higher than the flux saturation temperature to obtain the homogeneous liquid phase at the preliminary stage. Next, the temperature parameters of flux such as saturation temperature T_{sat} and metastable zone width ΔT_{met} are determined. At the growth stage, the crystal holder is inserted at a high temperature (comparable with the preparation and homogeneous liquid phase existence temperatures), and then, the temperature is rapidly decreased down to $T_{sat} - T_1$ ($T_1 > \Delta T_{met}$), at which point the crystallization occurs. If the super-cooled crystal holder is used (the crystal holder is inserted to the flux at a temperature below the saturation temperature), it is regarded as an external perturbation and the crystallization occurs even in the metastable zone. Usually, the super-cooled crystal holder is used to estimate the saturation temperature and metastable zone boundaries. For many systems, the crystallization in this mode is multiple and is not suitable for controllable growth of single crystals of high quality and sufficient size.

The flux system used to obtain $Cu_{1-x}Ni_xB_2O_4$ (x = 0.001 and 0.01) single crystals can be written in a quasi-binary form as follows:

$$(100 - n)\%\ \text{mass.}\ (Li_2WO_4 + pBi_2O_3 + qWO_3) + n\%\ \text{mass.}\ ((1 - x)CuO + xNiO + B_2O_3) \quad (1)$$

Due to the small amount of NiO oxide additives, at the initial stage, the properties of flux system (1) were studied at x = 0. The varying of q coefficient allows studying of the flux system in detail: the influence of WO_3 to saturation temperature, the width of the metastable zone and high temperature crystallizing phase type was determined. The influence of the temperature decreasing rate (at the stage of crystal growth) to the crystallization process was studied for several fluxes. The parameters of the flux system (1) are presented in Table 1.

The fluxes (1) have been prepared in a platinum crucible (V = 100 cm^3) at temperature T = 1000 °C by the sequential melting of oxides: first, the mixture of B_2O_3–Li_2WO_4–Bi_2O_3–WO_3 was melted, and then, CuO and NiO oxides were added in portions. The prepared fluxes were homogenized at the temperature T = 1000 °C for 3 h.

At the stage of temperature parameters of flux determination, the temperature in the furnace was decreased at a rate of $dT/dt \approx 100$ °C h^{-1} down to $T \approx T_{sat} - 2$ °C. After that, the crystal holder was inserted to the flux (before insertion, the crystal holder was preheated over the flux surface for 30 s). The crystal holder was extracted after t = 30 min, and the crystal formation was estimated. For each q, the saturation temperatures and type of high-temperature crystallizing phase were determined (Table 1).

The crystal formation was studied in four flux systems with different WO_3 contents (Table 1). The probing of fluxes using the insertion of the crystal holder at metastable zone temperatures showed metaborate-phase CuB_2O_4 as a high-temperature crystallizing phase for each of them. However, at the insertion of the crystal holder to the fluxes at the homogenization temperature T = 1000 °C and decreasing the temperature lower than $T_{sat} - T_1$ ($T_1 > \Delta T_{met}$), the other scenarios of phase formation have been observed.

The saturation temperatures, metastable zone width dependent on the rate of temperature lowering at the growth stage, and the type of high-temperature crystallizing phase are presented in Table 1. Experiments show the possibility of crystallization of other high-temperature crystallizing phases such as $LiBiW_2O_8$, Bi_2WO_6, and CuO besides CuB_2O_4, which could be obtained without using a super-cooled crystal holder. The metastable zone width (the difference between the saturation temperature and the temperature at the beginning of crystal formation in this case) of the studied fluxes to a high degree depends on the rate of temperature lowering – the rate of metastable zone boundary crossing. For instance, in the case of no. 2 parameter set (Table 2), the increasing of the lowering temperature rate from 5 to 10 °C per day, the difference between the saturation temperature and the temperature at the beginning of crystal formation increases twice: from 30 to 60 °C.

The working temperature range, including saturation temperatures and temperatures of crystal growth, is quite low and near to the temperatures of flux solidification (≈690 °C).

Table 1 Parameters of the flux system (1). q – weight coefficient of WO_3; dT/dt – cooling rate; n – concentration of crystal-forming oxides; ΔT_{met} – metastable zone temperature range; T_{sat} – saturation temperature; HTCP – high-temperature crystallizing phase obtained without super-cooled crystal holder (phase identification has been performed using powder X-ray diffraction and EDX)

No.	q	n, %	T_{sat}, °C	ΔT_{met}, °C	dT/dt, °C per day	HTCP
1	0.125	24	767	27	5	CuO
2	0.22	22.9	760	30	10	Simultaneous crystallization of Bi_2WO_6 and CuB_2O_4
				60	5	$LiBiW_2O_8$
3	0.313	21.9	768	33	10	CuB_2O_4 in a form of elongated prisms and plates localized at the surface of flux (Fig. 1c and d)
				53	5	Simultaneous crystallization of CuB_2O_4 and $LiBiW_2O_8$
4	0.501	20.2	792	57	10	CuB_2O_4 in a form of quadratic plates localized at the surface of flux (Fig. 1b)
				75	5	Simultaneous crystallization of CuB_2O_4 and $LiBiW_2O_8$

Table 2 Main parameters of processing and refinement of the CuB_2O_4:xNi samples

x (Ni)	Space group	Cell parameters (Å), cell volume (Å^3)	R_{wp}, R_p, R_B, χ^2
0.001	*I*-42*d*	a = 11.49780 (15), c = 5.62608 (8), V = 743.77 (2)	2.86, 2.22, 1.18, 1.58
0.01	*I*-42*d*	a = 11.49731 (9), c = 5.62593 (6), V = 743.681 (14)	2.69, 2.05, 1.384, 1.61
0.05	*I*-42*d*	a = 11.49639 (13), c = 5.62437 (7), V = 743.36 (2)	3.14, 2.44, 1.90, 1.39
0.1	*I*-42*d*	a = 11.49494 (17), c = 5.62372 (9), V = 743.08 (2)	3.54, 2.70, 1.84, 1.56

Despite this, the appreciable flux viscosity increase was observed only in the case of q = 0.125. Low working temperatures are the cause of the crystallization of $LiBiW_2O_8$ and Bi_2WO_6 phases containing the solvent components. The high solubility of the crystal-forming oxides (CuO and B_2O_3) in the used fluxes allows dealing with much greater concentrations in the future.

The significant difficulty in obtaining qualitative samples is the near-surface character of nucleation in CuB_2O_4 crystals in many fluxes including those used and known from the literature.[15–18] Besides the phase formation study using the traditional growth and super-cooled crystal holder, the distribution of metaborate crystals in the volume of flux in both modes was studied.

In the mode of inserting the crystal holder into the flux at homogenization temperatures in the cases of q_3 = 0.313 and q_4 = 0.501, the metaborate phase is the high-temperature crystallizing phase at a high cooling rate (10 °C per day). However, the habit of the obtained single crystals significantly differs from the one described in the literature, and the isometric crystals obtained using a super-cooled crystal holder can be explained by the fast crystal growth at high rates of temperature lowering at the growth stage. In the case of q_3 = 0.313, the obtained CuB_2O_4 single crystals were in a form of elongated prisms and plates (Fig. 1c and d), in the case of q_4 = 0.501 – thin quadratic plates (Fig. 1b). In both cases, the crystals were localized at the surface of flux. At a lower temperature change rate, the simultaneous formation of CuB_2O_4 and $LiBiW_2O_8$ took place due to the increase in metastable zone width.

The other scenarios of crystal formation were obtained using a super-cooled crystal holder – the crystal holder was inserted into the flux at the temperature of the metastable zone but not at the homogenization temperature. For all four systems described in Table 1, the high-temperature crystallizing phase was CuB_2O_4 metaborate using a super-cooled crystal holder. In this mode, crystal nucleation was observed not only in the near-surface zone but also in the volume of flux too. The varying of the q coefficient revealed the depth dependence of the mass distribution of crystals on the WO_3 concentration. At the lowest q_1 = 0.125, the distribution of crystals on the crystal holder was almost homogeneous, with slight mass transfer to the surface

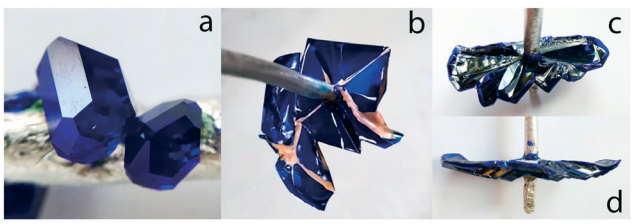

Fig. 1 Habit of CuB_2O_4 crystals, obtained under different conditions: a – super-cooled crystal holder is used, flux system no. 1 (Table 1); b – the crystal holder has been inserted to the flux at T = 1000 °C, flux system no. 4 (Table 1); c and d – the crystal holder has been inserted to the flux at T = 1000 °C, flux system no. 3 (Table 1).

(Fig. 2a). In some probing cases, the crystal formation was observed only in a volume. At the q coefficient, an increase in the mass transfer to a surface increases too (Fig. 2). At q_4 = 0.501, the crystal formation was observed only in the near-surface layer (Fig. 2d). Upon decrease in the weight of WO_3 in (1), the viscosity of flux increases. It can influence the flux depth distribution of the crystals (together with the change in flux density).

The study of crystal formation in the fluxes (1) in modes using a super-cooled crystal holder and the insertion of a crystal holder at the homogenization temperature made it possible to choose the most optimal scenario for the growth of qualitative volumetric single crystals of CuB_2O_4, with further substitutions of part of copper cations by nickel cations. To do this, system no. 2 (Table 1) was selected, corresponding to the value of the coefficient q_2 = 0.22. The crystal formation in this system remains volumetric and it does not have as high viscosity as system no. 1. Due to the high viscosity, at the crystal cooling stage after the growth stage (the crystal holder with grown crystals rises above the flux surface, and the furnace is cooled to room temperatures), the flux can flow poorly from the samples, thus provoking the additional formation of the crystals on the surface of grown ones, which spoils the quality of the faces.

The single crystals of $Cu_{1-x}Ni_xB_2O_4$ (x = 0.001, 0.01) were grown from flux no. 2 (see Table 1) using the following growing technique. After preparation of flux (1) (now with the appropriate additives NiO), the temperature in the furnace decreased at a rate of $dT/dt \approx 100$ °C h^{-1} to temperature (T_{sat} − 2) °C, and then, a crystal holder in the form of a platinum rod was inserted into the crucible with the flux. At a flux depth of 35 mm, the crystal holder was charged to 30 mm. After 30 min, the crystal holder was extracted and the following crystal formation was observed:

x = 0.001: two single crystals in the near-surface layer, one crystal at a distance of 12 mm from the bottom of the crucible, dimensions ~0.2 mm.

x = 0.01: one crystal at a distance of 5 mm from the bottom of the crucible, dimensions ~0.2 mm.

These crystals were used as seeds. The crystal holder was loaded into the flux at a temperature of $T = T_{sat}$ + 10 °C. After 10 min, the temperature in the furnace was reduced to (T_{sat} − 2) °C.

After insertion of the crystal holder with seeds into the flux, the temperature in the furnace was slowly decreased at a rate of dT/dt = 5 °C per day for 3 days. After the end of the growth stage, the crystal holder had risen above the flux. The grown single crystals cooled at a rate of 50 °C h^{-1}.

Powder X-ray diffraction

The powder diffraction data of CuB_2O_4:xNi (x = 0.001 and 0.01) for Rietveld analysis were collected at room temperature using a Bruker D8 ADVANCE powder diffractometer (Cu-Kα radiation) and a linear VANTEC detector. The step size of 2θ was 0.016°, and the counting time was 1 s per step. Almost all peaks, besides small impurity peaks (wt. ~1–2%) of SiO_2, were indexed by a tetragonal cell (I-42d) with parameters close to CuB_2O_4.[19] The impurity appeared after grinding CuB_2O_4 single crystals in an agate mortar. These structures were taken as starting models for Rietveld refinement, which was performed using TOPAS 4.2.[20] There are two Cu sites in the asymmetric part of the CuB_2O_4 unit cell, and both of them were occupied by Cu^{2+}/Ni^{2+} ions (Fig. 3) with a fixed ratio according to the suggested chemical formula. Refinements were stable and gave low R-factors (Table 2). The obtained data were compared with the same for earlier obtained CuB_2O_4:xNi (x = 0.05 and 0.1).[21] Linear cell volume dependence of $V(x)$ proves that suggested chemical compositions are close to the real ones (Fig. 4).

The crystallographic data are deposited in Cambridge Crystallographic Data Centre (CCDC # 2084362 and 2084363).

Infrared spectra

a. Experimental and fitting details

IR reflection and transmission spectra were measured using a Fourier spectrometer Bruker IFS 125HR. For reflection spectra, a special reflection attachment was used. To polarize the incident beam, a wire-grid and KRS-5 polarizers were used in the far-infrared (FIR, 10–700 cm^{-1}) and mid-infrared (MIR, 400–3000 cm^{-1}) spectral regions, respectively. A liquid-helium-cooled bolometer and liquid-nitrogen-cooled MCT

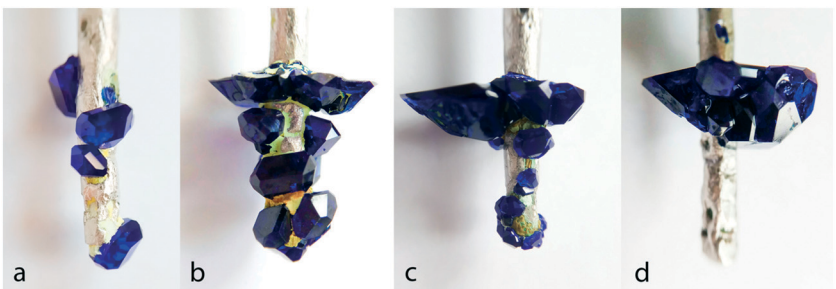

Fig. 2 Distribution of CuB_2O_4 crystals on the crystal holder depending on the q in fluxes (1), described in Table 1: a – no. 1, b – no. 2, c – no. 3, d – no. 4. Remark: yellow and light-green areas are remains of etched flux, it has not been fully removed to avoid the separation of the crystals from the crystal holder.

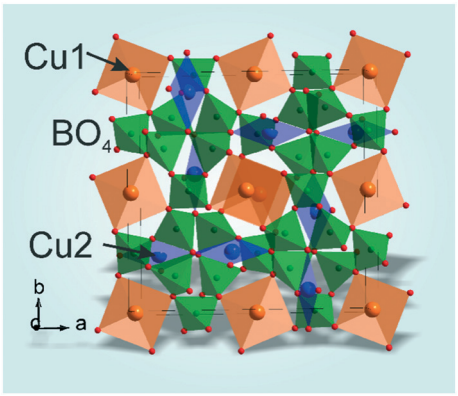

Fig. 3 Crystal structure of CuB_2O_4:*x*Ni.

detectors were used as detectors in the FIR and MIR regions, respectively, as well as DTGS and DLaTGS detectors. The obtained spectra were fitted using the RefFIT program.[22] This program uses the least square method and performs calculations according to eqn (2), in which frequency-dependent reflection coefficient $R(\omega)$ is expressed through the dielectric function $\varepsilon(\omega)$ as follows:

$$R(\omega) = \left| \frac{1 - \sqrt{\varepsilon(\omega)}}{1 + \sqrt{\varepsilon(\omega)}} \right|^2. \quad (2)$$

The complex dielectric function can be represented as the sum of N damped oscillators as follows:

$$\varepsilon(\omega) = \varepsilon_\infty + \sum_{j=1}^{N} \frac{f_j \omega_j^2}{\omega_j^2 - \omega^2 + i\gamma_j \omega}. \quad (3)$$

Here ω_j, f_j and γ_j are the frequency, oscillator strength, and damping constant for the j-th oscillator; ε_∞ is the dielectric constant at high frequencies.

b. Symmetry analysis of the lattice mode

The primitive cell of CuB_2O_4 contains 42 atoms. The symmetry analysis leads to the following distribution of the 126 phonon modes between the irreducible representations at the $\Gamma = 0$ point of the Brillouin zone:

$$126\Gamma = 13A_1(xx,yy,zz) + 17A_2 + 14B_1(xx,yy) + 18B_2(z,xy) + 32E(x,y,xz,yz) \quad (4)$$

Here $B_2(z,xy) + E(x,y,xz,yz)$ are acoustic modes, $17B_2(z,xy)$ and $31E(x,y,xz,yz)$ are polar modes, $13A_1(xx,yy,zz)+ 14B_1(xx,yy)$ are Raman-active modes, and $17A_2$ modes are silent. Detailed symmetry analysis can be found in ref. 23.

c. Infrared transmission and reflection spectra

Fig. 5 shows the room-temperature reflection spectra of $Cu_{1-x}Ni_xB_2O_4$: x = 0.001 (a) and 0.01 (b), registered for the polarization of the incident light $E(\omega)\|z$, in which, according to the symmetry analysis, 31 modes $E(x,y)$ should be observed. The corresponding spectra for the polarization $E(\omega)\|z$ (17 modes $B_2(z)$) are shown in Fig. 6(a and b). The

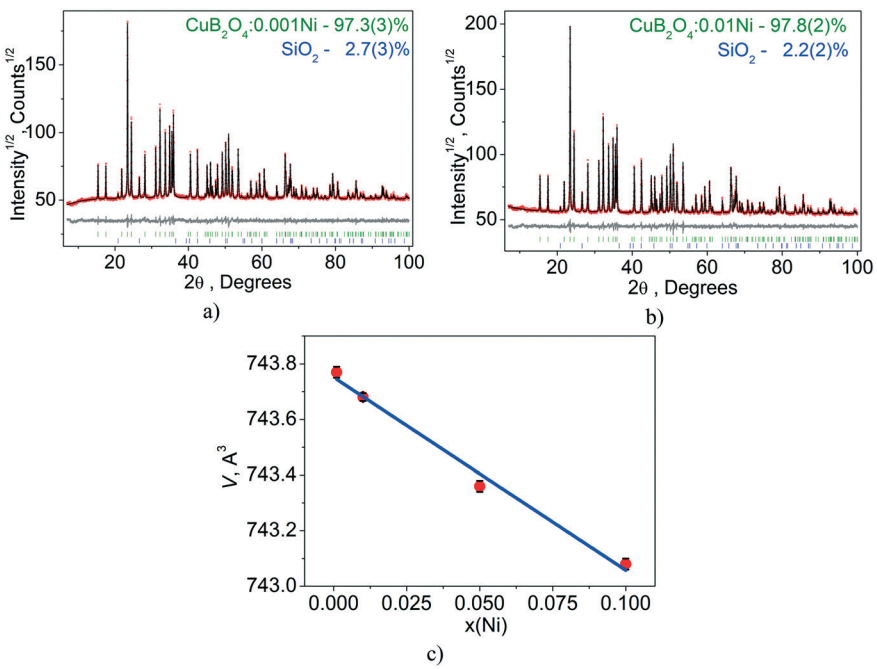

Fig. 4 Difference Rietveld plot of CuB_2O_4:*x*Ni: a) x = 0.001 and b) x = 0.01. Linear cell volume dependence $V(x)$ (c). Symmetry codes: (i) $-x + 1/2$, y, $-z + 3/4$; (ii) $-y$, $-x + 1/2$, $z - 3/4$; (iii) x, y, $z - 1$; (iv) $-y$, $-x + 1/2$, $z + 1/4$; (v) $-y$, x, $-z + 1$.

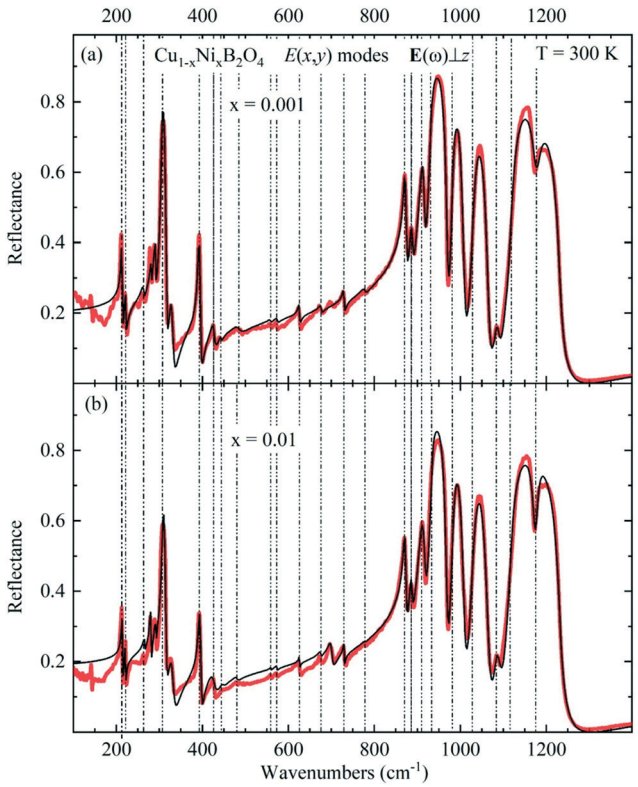

Fig. 5 $E(\omega)||x,y$-polarized room-temperature infrared reflection spectra (thick red lines) of $Cu_{1-x}Ni_xB_2O_4$: x = 0.001 (a) and 0.01 (b), measured with the polarization of the incident light $E(\omega)||z$. Spectra are compared with fitting calculations (thin black lines) based on a model of damped oscillators. Vertical dashed lines show frequencies (TO) obtained from fitting.

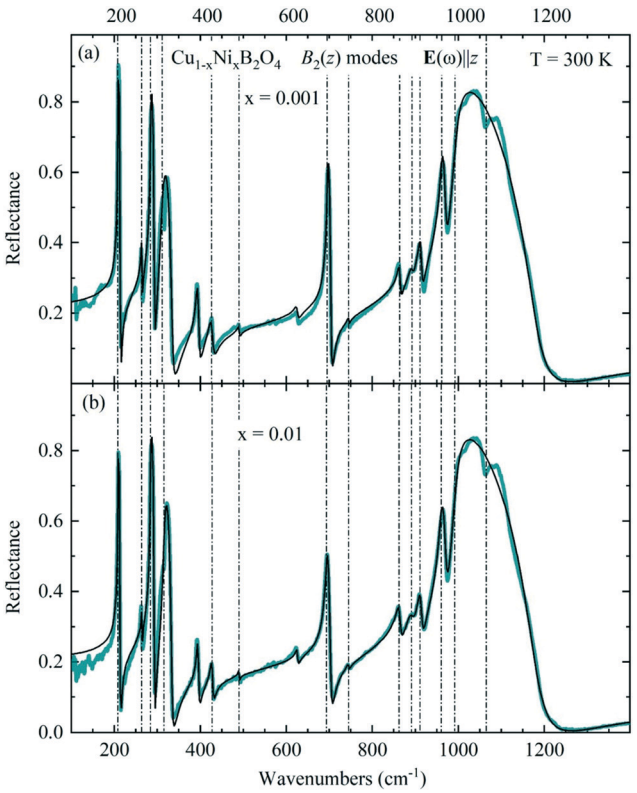

Fig. 6 $E(\omega)||z$-polarized room-temperature infrared reflection spectra (thick cyan lines) of $Cu_{1-x}Ni_xB_2O_4$: x = 0.001 (a) and 0.01 (b). Spectra are compared with fitting calculations (thin black lines) based on a model of damped oscillators. Vertical dashed lines show frequencies (TO) obtained from fitting.

parameters of the phonon modes were obtained from fitting the spectra using the RefFit[22] program. For convenience in comparing the spectra, the TO frequencies are marked by the vertical dash-dotted lines. In order to reveal weak, poorly distinguishable modes in the reflection spectra, the temperature dependence of the unpolarized transmission spectra (5–300 K) of $Cu_{1-x}Ni_xB_2O_4$ (x = 0.01) was also recorded. The frequencies of the phonon modes of $Cu_{1-x}Ni_xB_2O_4$ do not practically depend on the temperature (the same character was observed for CuB_2O_4 (ref. 22)); therefore, we present the spectrum only at the lowest temperature T = 5 K as the most illustrative one (Fig. 7). The arrows indicate the modes observed only in the transmission spectra.

In total, 30 out of 31 $E(x,y)$ modes and all 17 $B_2(z)$ modes were registered. The frequencies of all observed modes are summarized in Tables 3 and 4 in comparison with the corresponding frequencies of CuB_2O_4 (x = 0) published in.[23] As can be seen from the figures and the tables, TO frequencies of $Cu_{1-x}Ni_xB_2O$ for x = 0, 0.001, and 0.01, obtained from reflection spectra fitting, are practically equal for both polarizations. The difference $\Delta\omega$ (TO) is about 1 cm^{-1} for the majority of modes and associated with the fitting error. At the same time, TO frequencies of the lowest modes obtained from the transmission spectra were determined with higher accuracy. Thus, ω_{TO} = 143.2 cm^{-1}, 191.6 cm^{-1} ($E(x,y)$ modes) and 151.2 cm^{-1} ($B_2(z)$ modes) for $Cu_{1-x}Ni_xB_2O_4$, while the corresponding CuB_2O_4 TO frequencies are 140 cm^{-1}, 190 cm^{-1} ($E(x,y)$) and 150 cm^{-1}($B_2(z)$). The increase in the frequency of the lowest-lying modes associated with the 3d

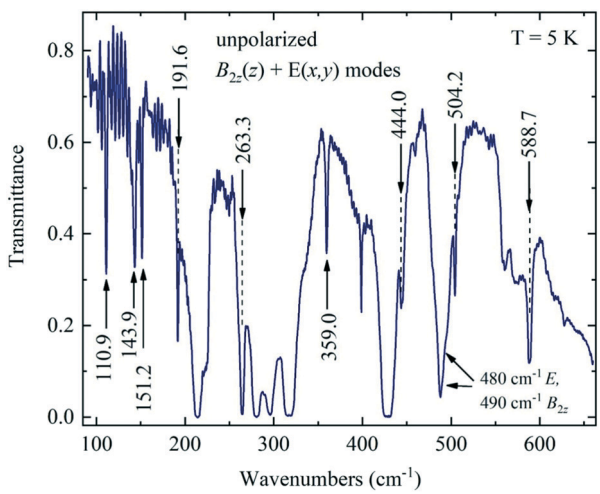

Fig. 7 Unpolarized transmission spectra of $Cu_{1-x}Ni_xB_2O_4$ (x = 0.01) at T = 5 K. The arrows show the weak modes indistinguishable on reflection spectra.

Table 3 Frequencies of the observed $E(x,y)$ polar modes of $Cu_{1-x}Ni_xB_2O_4$ (x = 0.001 and 0.01) single crystals expressed in cm^{-1} in comparison with the corresponding frequencies of CuB_2O_4 (ref. 23)

	Frequency (TO)ω_j, cm^{-1}		
j	x = 0.01	x = 0.001	x = 0 (ref. 23)
1	143.2[a]		142.0[a]
2	191.6[a]		190.0[a]
3	212.7	212.2	212.4
4	221.5	221.4	221.0
5	263.3[a]	263.0	263.1[a]
6	279.0	280.1	278.8
7	307.1	304.7	302.2
8	359.0[a]		360.0[a]
9	392.8	391.3	390.0
10	425.3	426.1	426.1
11	444.0[a]	443.0	444.0[a]
12	480	485	479.6[a]
13	504.2[a]		503.0[a]
14	559.0	558.0	558.9[a]
15	573.0	574.2	573.0[a]
16	625.7	625.6	625.0
17	675.0	675.9	676.2
18	729.6	729.4	729.3
19	777.7	778.2	778.8[a]
20			796.0[a]
21	870.2	870.0	869.8
22	885.9	886.3	886.2
23	910.2	909.4	908.3
24	933.1	931.0	929.0
25	981.6	980.7	979.4
26	1028.0	1028.5	1027.9
27	1083.9	1083.9	1083.0
29	1115.4	1118.5	1122.3
30	1175.4	1177.0	1176.5

[a] Observed in transmission spectra.

Table 4 Frequencies of the observed $B_2(z)$polar modes of the $Cu_{1-x}Ni_xB_2O_4$ (x = 0.001 and 0.01) single crystals expressed in cm^{-1} in comparison with the corresponding frequencies of CuB_2O_4 (ref. 23)

	Frequency (TO)ω_j, cm^{-1}		
j	x = 0.01	x = 0.001	x = 0 (ref. 23)
1	110.9[a]		110[a]
2	151.2[a]		150[a]
3	208.2	207.8	207.7
4	263.9	263.5	263.2
5	284.1	284.5	282.6
6	315.5	311.2	317.0
7	427.2	425.9	427.7
8	490	490	490.5
9	588.7[a]	—	587.9[a]
10	693.1	694.8	693.9
11	744.8	745.1	744.8
12	862.5	863.5	863.1
13	891.5	892.2	894.2
14	911.2	911.6	911.4
15	960.2	961.5	963.9
16	991.7	992.6	995.9
17	1065.0	1065.0	1063.8

[a] Observed in transmission spectra.

ion (Cu, Ni) vibrations is most likely due to the fact that the mass of Cu^{2+} exceeds the mass of Ni^{2+} (63,54 *vs.* 58,69).

Conclusions

This paper presented the results of the work on growing single crystals of $Cu_{1-x}Ni_xB_2O_4$ metaborate by a flux method using a Li_2O–WO_3–Bi_2O_3–WO_3 solvent, previously not used for the synthesis of these compounds. The crystal formation pattern in flux system (1) is very complex due to the simultaneous influence of many factors. All the fluxes (1) have a wide metastable zone, the determination of the zone width being highly dependent on the cooling rate of the flux on the growth stage (Table 1). With the increase in the rates of temperature lowering to 10 °C per day, the width of the metastable zone decreases.

For part of the studied fluxes in the mode of a crystal holder inserted at high temperatures, the high-temperature CuB_2O_4 phase is not stable: other compounds are formed from the components of the flux with the composition sensitive to mass fraction WO_3; simultaneous crystallization of two phases including the occurrence of the metaborate phase.

The effect of tungsten oxide on the distribution of metaborate nucleation in the depth of the flux was studied by varying the coefficient q in (1). As in other works using various solvents, there was a tendency to form single crystals of the metaborate in the near-surface layer. However, changing the mass fraction of WO_3 qualitatively transforms the pattern of crystal formation due to the influence on the viscosity of the flux at working temperatures of T = 700 ÷ 780 °C. With the highest content of WO_3 (no. 4, Table 1), the crystal formation of CuB_2O_4 was observed mainly in the near-surface layer. With a decrease in the fraction of WO_3, there is a tendency to form crystals in the volume, along with near-surface formation.

Throughout the study, the flux system with optimal parameters for obtaining volumetric high-quality single crystals of $Cu_{1-x}Ni_xB_2O_4$ (x = 0.001 and 0.01) in a mode of nucleation in metastable zone using a super-cooled crystal holder was determined. Powder X-ray analysis of the obtained samples as well as the comparison with the structural data of $Cu_{1-x}Ni_xB_2O$ metaborate with x = 0.05 and 0.1 was obtained earlier, which showed the linear dependence of the unit cell volume on the concentration x taken in the flux. It indicates the proximity of x to the real composition. Infrared reflection and transmission spectra of the synthesized single crystals were measured and analyzed in comparison with "pure" CuB_2O_4. Despite the low nickel concentration, its presence in $Cu_{1-x}Ni_xB_2O_4$ (x = 0.001 and 0.01) is reflected in the obtained spectra, as the increase in frequencies of the lowest frequency phonons is associated with 3*d* ion vibrations, which gives a perspective to further study the optical properties.

Conflicts of interest

There are no conflicts to declare.

Acknowledgements

The authors acknowledge Dr. Irina Gudim regarding the valuable discussion of the obtained results on the

experimental stage and the stage of manuscript preparation. This research was supported by the Russian Science Foundation grant no.19-12-00413. X-ray and EDX data was obtained with use the analytical equipment of Krasnoyarsk Regional Center of Research Equipment of Federal Research Center "Krasnoyarsk Science Center SB RAS".

References

1 W. Guertler, About the Oxygen Evolution from Cupric m-Borate, *Z. Anorg. Chem.*, 1904, **38**, 456–460.
2 W. Guertler, Crystallization of glassy masses, *Z. Anorg. Chem.*, 1904, **40**, 268–279.
3 A. D. Molchanova and K. N. Boldyrev, High-Resolution Spectroscopy of Low-Temperature Phase Transitions in Copper Metaborate CuB_2O_4, *Opt. Spectrosc.*, 2019, **127**(1), 33–35.
4 E. N. Ovchinnikova, A. Rogalev, F. Wilhelm, K. A. Kozlovskaya, A. P. Oreshko and V. E. Dmitrienko, X-Ray Natural Circular Dichroism in Copper Metaborate, *J. Exp. Theor. Phys.*, 2016, **123**(1), 27–32.
5 K. N. Boldyrev, R. V. Pisarev, L. N. Bezmaternykh and M. N. Popova, Antiferromagnetic Dichroism in a Complex Multisublattice Magnetoelectric $CuB_{(2)}O_{(4)}$, *Phys. Rev. Lett.*, 2015, **114**(24), 247210.
6 M. Saito, K. Taniguchi and T. Arima, Gigantic Optical Magnetoelectric Effect in CuB_2O_4, *J. Phys. Soc. Jpn.*, 2008, **77**(1), 013705.
7 S. Toyoda, N. Abe, S. Kimura, Y. H. Matsuda, T. Nomura, A. Ikeda, S. Takeyama and T. Arima, One-way transparency of light in multiferroic CuB_2O_4, *Phys. Rev. Lett.*, 2015, **115**, 267207.
8 S. Toyoda, N. Abe and T. Arima, Nonreciprocal refraction of light in a magnetoelectric material, *Phys. Rev. Lett.*, 2019, **123**, 77401.
9 S. Toyoda, M. Fiebig, T. Arima, Y. Tokura and N. Ogawa, Nonreciprocal second harmonic generationin a magnetoelectric material, *Sci. Adv.*, 2021(7), eabe2793.
10 D. Kudlacik, V. Yu. Ivanov, D. R. Yakovlev, V. F. Sapega, J. J. Schindler, J. Debus, M. Bayer and R. V. Pisarev, Exciton and exciton-magnon photoluminescence in the antiferromagnet CuB_2O_4, *Phys. Rev. B*, 2020, **102**, 035128.
11 N. Anantharamulu, B. V. Kumar, V. R. Devi, T. Sarojini, Ch. Anjaneyyulu and M. Vithal, Preparation and characterization studies of metaborates, $Cu_{1-x}M_xB_2O_4$ (M = Ni, Co and Mn; x = 0, 0.1 and 0.5), *Bull. Mater. Sci.*, 2009, **32**(4), 421–430.
12 A. D. Molchanova, K. N. Boldyrev, A. S. Erofeev, E. M. Moshkina and L. N. Bezmaternykh, Magnetic phase transitions and linear magnetic dichroism in manganese-doped copper metaborate $(Cu,Mn)B_2O_4$, *J. Phys.: Conf. Ser.*, 2017, **917**, 072003.
13 N. D. Khanh, N. Abe, K. Kubo, M. Akaki, M. Tokunaga, T. Sasaki and T. Arima, Magnetic control of electric polarization in the noncentrosymmetric compound $(Cu,Ni)B_2O_4$, *Phys. Rev. B: Condens. Matter Mater. Phys.*, 2013, **87**, 184416.
14 M. Saito, K. Ishikawa, S. Konno, K. Taniguchi and T. Arima, Periodic rotation of magnetization in a non-centrosymmetric soft magnet induced by an electric field, *Nat. Mater.*, 2009, **8**(8), 634–638.
15 L. Lecuir and J. Guillermet, Fritting preparation and characterization of two borates, CuB_2O_4 and $Cu_3B_2O_6$, *C. R. Seances Acad. Sci., Ser. B*, 1971, **273**(25), 1091–1094.
16 G. A. Petrakovskii, K. A. Sablina, D. A. Velikanov, A. M. Vorotynov, N. V. Volkov and A. F. Bovina, Synthesis and magnetic properties of copper metaborate single crystals, CuB_2O_4, *Kristallografiya*, 2000, **45**(5), 926–929.
17 L. N. Bezmaternykh, E. A. Varganova, A. D. Vasil'ev, I. A. Gudim and V. L. Temerov, Growth and structure study of copper borate single crystal, *Poverkhn.: Rentgenovskie, Sinkhrotronnye Neitr. Issled.*, 2002(5), 37–39.
18 L. N. Bezmaternykh, S. V. Beluschenko and I. A. Gudim, Crystallization of copper borates in Bi_2O_3-B_2O_3-MoO_3-CuO flux, *Poverkhn.: Rentgenovskie, Sinkhrotronnye Neitr. Issled.*, 2004(9), 5–7.
19 G. K. Abdullaev and K. S. Mamedov, Refined crystal structure of copper metaborate CuB_2O_4, *J. Struct. Chem.*, 1981, **22**(4), 637–639.
20 Bruker AXS, *TOPAS V4: General profile and structure analysis software for powder diffraction data. – User's Manual*, Bruker AXS, Karlsruhe, Germany, 2008.
21 E. Moshkina, A. Molchanova, K. Boldyrev, M. Molokeev and A. Bovina, Synthesis and properties of copper metaborate crystals doped by nickel and manganese, *Opt. Spectrosc.*, 2021, in press.
22 A. B. Kuzmenko, Kramers-Kronig constrained variational analysis of optical spectra, *Rev. Sci. Instrum.*, 2005, **76**, 083108.
23 R. V. Pisarev, K. N. Boldyrev, M. N. Popova, A. N. Smirnov, V. Yu. Davydov, L. N. Bezmaternykh, M. B. Smirnov and V. Yu. Kazimirov, Lattice dynamics of piezoelectric copper metaborate CuB_2O_4, *Phys. Rev. B: Condens. Matter Mater. Phys.*, 2013, **88**, 024301.

